Medicinal Chemistry Research (2019) 28:820–830
https://doi.org/10.1007/s00044-019-02311-x

MEDICINAL CHEMISTRY RESEARCH

ORIGINAL RESEARCH

3D-QSAR modeling of Phosphodiesterase-5 inhibitors: evaluation and comparison of the receptor- and ligand-based alignments

Zan Jiang[1] · Xuehua Zheng[2] · Zhong Li[1] · Shuqiong Pan[2] · Xiaoyu Wang[2] · Chen Zhang[3] · Zhe Li[3] · Hai-Bin Luo[3] · Deyan Wu[3] · Xiong Cai[1]

Received: 1 November 2018 / Accepted: 6 February 2019 / Published online: 16 April 2019

Abstract

Phosphodiesterase-5 (PDE5) inhibitors can be used as clinical agents for the treatment of erectile dysfunction and pulmonary hypertension. A series of aryl-chromeno-pyrrol derivatives were previously identified as PDE5 inhibitors in our lab. Herein, these molecules were subjected to 3D-QSAR analysis with CoMFA and CoMSIA methods to gain deeper insight into the structural requirements for their bioactivities. Receptor- and ligand-based alignment were used and compared to find the alignment-related factors that affect the accuracy of QSAR models. The receptor-based CoMFA and CoMSIA models, which were generated by superimposing the docking conformations directly in the protein binding site, gave more significant results for 38 training set compounds and 5 test set molecules. Comparison of the two alignments revealed that spatial arrangement of the ligands is the principal factor in determining the reliability of the 3D-QSAR models. Detailed analysis of the receptor-based CoMSIA-SE contour maps provided much helpful information to improve the bioactivities of aryl-chromeno-pyrrol analogs as PDE5 inhibitors.

Keywords: Phosphodiesterase · PDE5 inhibitor · 3D-QSAR · CoMFA · CoMSIA

Introduction

Phosphodiesterase type 5 (PDE5), one of the 11 families of PDEs, plays a critical role in regulating cGMP levels by catalyzing the breakdown of cGMP into 5′-GMP (Francis et al., 2011). PDE5 is highly expressed in smooth muscles of lungs and the corpus cavernosum (Champion et al., 2005; Corbin et al., 2005). Inhibition of PDE5 increases the level of cGMP, which can activate downstream proteins to eventually cause muscle relaxation and vasodilation. PDE5 inhibitors have served as drugs for the treatment of male erectile dysfunction (ED) and pulmonary hypertension (PH) (Unegbu et al., 2017; Scaglione et al., 2017). Moreover, applications of PDE5 inhibitors against several diseases associated with low cGMP levels have also been reported (Ribaudo et al., 2016; Andersson, 2018). Currently, there are several clinically used PDE5 inhibitors for chronic treatment of most ED cases such as sildenafil, vardenafil, tadalafil, avanafil, udenafil, and mirodenafil (Oh et al., 2000; Sakamoto et al., 2014; Jung et al., 2008; Keating and Scott, 2003; Rotella, 2002). Sildenafil and tadalafil have also been approved for the treatment of PH (Kuschner, 2005; Udeoji and Schwarz, 2013). However, several side effects have been identified in the use of PDE5 inhibitor therapy, including facial flushing, headaches, dyspepsia, nasal congestion, and dizziness together with blurred vision (Unegbu et al., 2017; Azzouni and Abu, 2011; Khan et al., 2011). Therefore, there has still remarkable interest in the development of novel PDE5 inhibitors with new scaffolds.

We previously discovered a series of 1-aryl chromeno [2,3-c]pyrrol-9(2H)-ones as potent PDE5 inhibitors (Shang et al., 2014; Wu et al., 2017). The crystal studies revealed that these compounds occupy the same pocket as other

✉ Xuehua Zheng
zhengxh23@gzhmu.edu.cn
Deyan Wu
wudeyan3@mail.sysu.edu.cn
Xiong Cai
caix12@qq.com

[1] School of Chinese Materia Medica, Guangdong Pharmaceutical University, Guangzhou 510006, China

[2] Key Laboratory of Molecular Target & Clinical Pharmacology, School of Pharmaceutical Sciences & the Fifth Affiliated Hospital, Guangzhou Medical University, Guangzhou 511436, China

[3] School of Pharmaceutical Sciences, Sun Yat-sen University, Guangzhou 510006, China

PDE5 inhibitors, but have a different binding pattern in detail (Shang et al., 2014). The obtained desirable inhibitory potency, selectivity, and pharmacokinetic properties indicate that it can be proposed as a novel scaffold of PDE5 inhibitors. In the present study, to provide more information for structural optimization of PDE5 inhibitors to further improve their binding affinities, three-dimensional quantitative structure activity relationship (3D-QSAR) studies have been carried out on 43 1-aryl chromeno[2,3-c]pyrrol-9 (2H)-ones by using comparative molecular field analysis (CoMFA) and comparative molecular similarity indices analysis (CoMSIA) approaches. To find out an effective alignment for this data set, receptor-, and ligand-based alignment were used to align the ligands for model building and external validation. The former superimposed the best-docked poses of the ligands directly in the protein-binding site, whereas the latter aligned the energy-minimized conformations of the ligands on the template using the traditional atom-fit technique. Then, superimposition effect and statistics results of the derived models were compared and evaluated to explore the alignment related factors affecting the reliability of the QSAR models. The obtained 3D-QSAR models with the aid of their 3D contour maps would facilitate the design and optimization of novel PDE5 inhibitors.

Materials and methods

Data sets for analysis

The 43 compounds were synthesized and evaluated for their biological activities in our laboratory, and can be classified into two series according to the substituents at the C3-position: alkyl substituent (**1**–**20**, group A) or aromatic ring (**21**–**43**, group B) (Shang et al., 2014; Wu et al., 2017). Their biological activities were converted into pIC_{50} (-log IC_{50}) values for the 3D-QSAR studies, which spread of a wide range from 5.000 to 8.268. The training and test sets were selected based on diversity principle that is both sets could completely cover the whole range of structural diversity and biological activity. Thus, the compounds were divided into five groups based on pIC_{50} values, and five test set compounds were selected from various biological and chemical sub-classes. The chemical structures and biological activities of the training and test set molecules are listed in Table 1, and compound **1**, **8**, **19**, **31**, and **35** included in the test set were marked with asterisk.

Molecular docking studies

Molecular docking was performed using CDOCKER module embedded in Accelrys Discovery Studio 2.5.5 (Discovery Studio 2.5.5, 2009). The crystal structure of PDE5A with molecule **26** bound (PDB entry code 4MD6) was used in this study as the receptor. All the water molecules were removed, while zinc and magnesium were allowed to remain with a charge of +2. A spherical region with a radius of 10 Å was constructed as the binding site, based on the location of the co-crystallized ligand. All the ligands and receptor were typed with CHARMm force field and Momany-Rome partial charges calculation method. Other input parameters were set as their default options. The original ligand **26** was docked back into the X-ray protein to verify the dock procedure. An RMSD less than 1.0 Å between the crystal and docked conformations was considered desirable docking protocol. Following these procedures, all the prepared ligands were docked into the active site of PDE5 using the identical parameters.

Alignment of dataset

As structural alignment is one of the most pivotal steps in the construction of 3D-QSAR models, the ligand alignments were achieved by two different methods.

Receptor-based alignment (RBA): The docking poses of the ligands were directly used to build CoMFA and CoMSIA models. Docking studies were performed as depicted above. The poses used for the QSAR studies were selected manually based on the docking scores and conformational similarities to the crystal pose of **26**. These poses were then transferred to a SYBYL database, clustered and assigned with Gasteiger-Marsili charges in the binding pocket of the receptor for a directly use in construction of QSAR models.

Ligand-based alignment (LBA): All compounds in the training and test set were aligned to the template compound **26** with rigid body alignment depending on the common substructures using SYBYL7.3.3 molecular modeling package (Sybyl7.3, 2006). The chemical structures of the ligands were optimized using Gasteiger–Marsili partial atomic charges, Tripos force field, and Powell's conjugate gradient method with 0.005 kcal/mol energy convergence criterion and 1000 maximum iterations. Common substructures were defined without including atom types and bond types in rings by Distill.

CoMFA and CoMSIA analysis

The CoMFA and CoMSIA analysis were performed using SYBYL7.3.3 software package. During the calculations of CoMFA and CoMSIA fields, a 3D cubic lattice with grid spacing of 2.0 Å was generated automatically. CoMFA steric and electrostatic fields at each lattice point were evaluated using an sp3 carbon atom probe carrying a + 1 net charge, and the energy exceeding 30 kcal/mol was ignored. CoMSIA physicochemical properties, which

Table 1 Structures, actual and predicted activities of the molecules in the training and test set

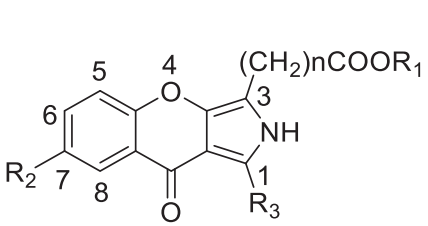

1-17

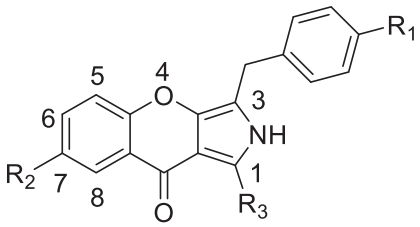

21-40

Cpd.	R_1(n)	R_2	R_3	pIC_{50}[a]		
				Actual	Predicted	Residual[b]
1*	-C(CH3)3 (n=1)	-CH3	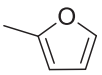	6.351	6.815	-0.464
2	-C(CH3)3 (n=1)	-OCH3	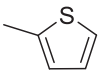	6.914	6.461	0.453
3	-C(CH3)3 (n=1)	-H	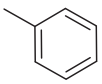	6.419	6.841	-0.422
4	-C(CH3)3 (n=1)	-H	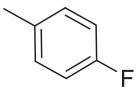	6.664	6.626	0.038
5	-C(CH3)3 (n=1)	-CH3	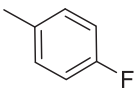	6.308	6.649	-0.341
6	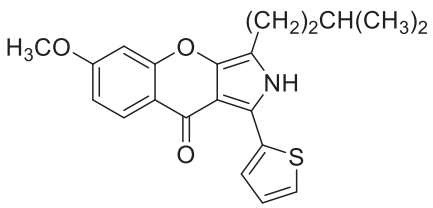			6.078	6.246	-0.168
7	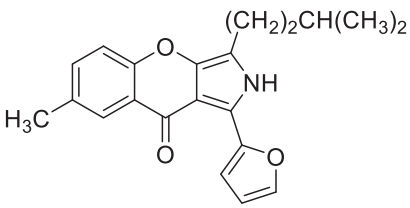			6.240	6.613	-0.373
8*	-H (n=2)	-OCH3	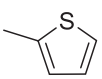	5.380	5.267	0.113
9	-H (n=2)	-Br	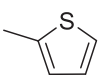	5.550	5.774	-0.105

10	-H (n=2)	-H	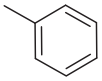	5.000	5.312	-0.312
11	-H (n=2)	$-CH_3$	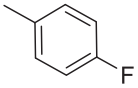	5.335	4.999	0.336
12	$-C(CH_3)_3$ (n=2)	$-OCH_3$	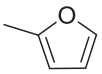	5.359	5.414	-0.055
13	$-C(CH_3)_3$ (n=2)	$-CH_3$	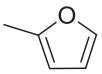	5.778	5.886	-0.108
14	$-C(CH_3)_3$ (n=2)	-H	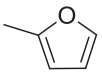	5.684	5.804	-0.120
15	$-C(CH_3)_3$ (n=2)	-Br	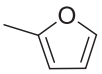	6.085	5.847	0.238
16	$-C(CH_3)_3$ (n=2)	$-OCH_3$	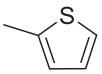	5.718	5.652	0.066
17	$-C(CH_3)_3$ (n=2)	-H	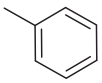	5.669	5.624	-0.074
18	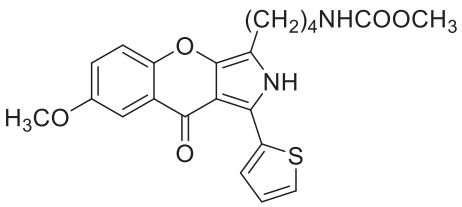			5.609	5.607	0.002
19*	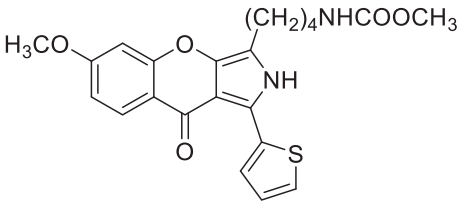			5.000	5.086	-0.086
20	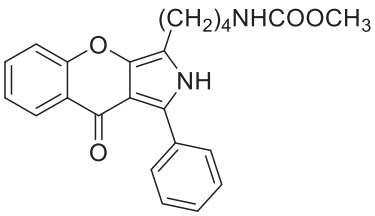			5.000	4.990	0.010
21	$-OC(CH_3)_3$	$-CH_3$	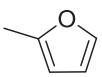	6.620	6.691	-0.071
22	$-OC(CH_3)_3$	-H	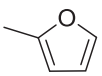	5.700	5.588	0.112
23	$-OC(CH_3)_3$	$-OCH_3$	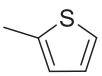	5.000	4.905	0.095

24	-H	-H	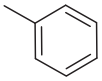	7.114	6.866	0.248
25	-H	-H	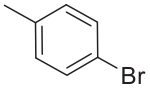	6.496	6.386	0.110
26	-OH	-H	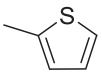	7.770	7.377	0.393
27	-OH	$-OCH_3$	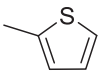	7.215	6.994	0.221
28	-OH	-Br	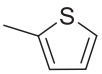	6.870	7.271	-0.401
29	-OH	-H	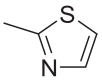	8.268	8.183	0.085
30	-OH	-H	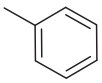	7.745	7.118	0.627
31*	-OH	-H	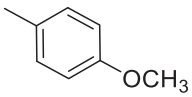	6.656	6.825	-0.169
32	-OH	$-CH_3$	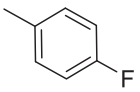	6.449	6.927	-0.478
33	-OH	-H	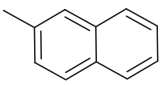	6.341	6.368	-0.027
34	-OH	-H	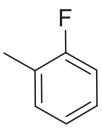	7.796	7.476	0.320
35*	-OH	-H	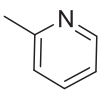	7.678	7.581	0.097
36	-OH	-H	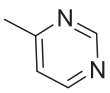	7.252	7.197	0.055
37	-OH	-H	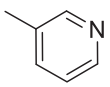	7.114	7.201	-0.087
38	-OH	-H	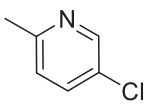	7.301	7.215	0.086

39	-OH	-H	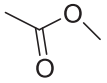	7.509	7.878	-0.369
40	$-CF_3$	-H	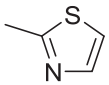	7.523	7.420	0.103
41			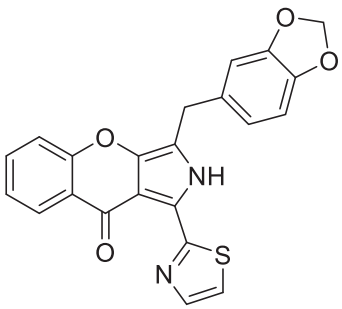	8.252	8.260	-0.008
42			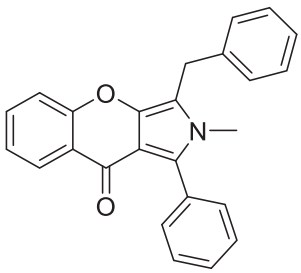	6.045	6.094	-0.049
43			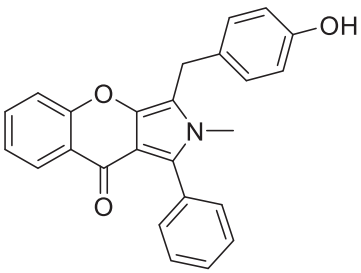	6.863	6.894	-0.031

*Compounds used in the test set

[a]$pIC_{50} = -\log IC_{50,}$ and IC_{50} was in M

[b]$\text{Residual} = pIC_{50(\text{actual})} - pIC_{50(\text{predicted})}$

include steric (S), electrostatic (E), hydrophobic (H), hydrogen bond donor (D), and acceptor (A) fields, were calculated using a probe of charge +1, hydrophobicity and hydrogen bonding properties of +1, and attenuation factor of 0.3.

Partial least square (PLS) regression analyses were employed to linearly correlate the pIC_{50} values (dependent variables) to CoMFA and CoMSIA fields (independent variables). Leave one out (LOO) cross-validation was firstly employed to produce the cross-validated correlation coefficient (q^2) and optimal number of components (ONC), in which one compound is excluded from the data set and its pIC_{50} value is estimated using the model derived from the rest. Using the optimal number of components, non-cross-validation with a column filter value of 1.0 kcal/mol was then performed to establish the final 3D-QSAR model, in which conventional correlation coefficient (r^2), standard error of estimate (SEE), and the *F*-test value (*F*) were calculated.

To further evaluate the robustness of the derived 3D-QSAR models, the biological activities for the test set, which comprise 5 molecules never used in the model building, were predicted to generate the predictive

correlation coefficient (q^2_{pred}), the conventional correlation coefficient (r^2_{pred}), and the trend line slope (k).

Results and discussion

Molecular docking and alignment

CoMFA and CoMSIA are the most commonly used 3D QSAR techniques to correlate the biological activities with structural changes of the ligands. Molecular alignment of the ligands including position, rotation, and conformation plays an important role in determining the accuracy of these approaches, because CoMFA and CoMSIA fields for the ligands were calculated based on their structure. By introducing receptor information during the alignment process, the so called receptor-based 3D-QSAR analysis, which uses the receptor bound ligands for model generation, has been proved to be more reliable (Zheng et al., 2016; Zheng et al., 2017; Tan et al., 2017). Thus, a receptor-based alignment (RBA) was used to generate 3D-QSAR models in the present study. The receptor bound pose of each compound was generated by docking it into the active site of PDE5A. To verify the docking procedure, the original ligand **26** of 4MD6 was re-docked into the X-ray protein. The RMSD between the docked and experimental conformations was found to be 0.1860 Å that means the present docking strategy was reliable in generation of PDE5 bound conformation for the ligands (Fig. 1a). Then, molecules in the training and test sets were successfully docked into the active site, and poses with reasonable scores and conformations in agreement with the crystallographic data were taken and aligned in the binding pocket of the receptor for a directly use to construct QSAR models. Result of the superimposed image of 43 compounds within the active site of PDE5 is shown in Fig. 1b.

As proposed by Li et al., the ligand-binding pocket of PDE5 can be divided into three major subsites: a metal-binding site (the M site), a core pocket (the Q pocket), and a solvent pocket (the S pocket) (Li et al., 2016). The complex crystal structure revealed that, in general, compound **26** is bound to PDE5A with the pyrrol of the core heading to the Q pocket of the bottom and the benzene ring of the core face to the entrance of active site (the S pocket). The aryl-chromeno-pyrrol core is sandwiched by Phe820 on one side and Val782 on the other side from the Q pocket, while the amine on the core forms a hydrogen bond with Q pocket Gln817, both of which are characteristically present in the binding of many PDE5 inhibitors. The pyrrol of the core brings the tyrosyl and thiophen substitutes on it, respectively, entering the deep part of the Q and M site in a "butterfly" shape. The tyrosyl group interacts with one of the hydrophobic subpocket (Q2) of the Q site, which is composed of hydrophobic residues of Val782, Ala783, Phe787, Ile813, and Met816. The thiophen ring forms hydrophobic interactions with residues of Ala767, Ile768, Gln775, and Ile778 from the subpocket of M site (SP1), in addition to the H-bond with the amide nitrogen of Gln817. Visual inspections of the best-docked geometries of all the compounds showed that active aryl-chromeno-pyrrol analogs ($IC_{50} < 1$ μM, $pIC_{50} < 6$) would generally mimic the binding pattern of compound **26** with substituent on C3-position entering the Q2 subpocket and substituent on C1-position occupying the SP1 subpocket of M site. However, too long substituents on the pyrrol C3-position could not be accommodated by the Q2 subpocket, thus leading to the

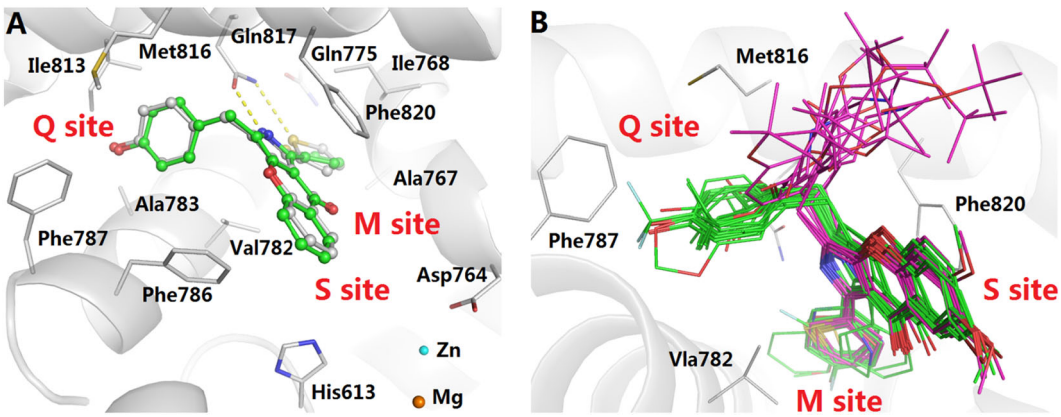

Fig. 1 Results of molecular docking and receptor-based alignment. **a** Validation of the molecular docking procedures by comparison of the crystal (stick and ball, gray-carbon, 4MD6) and docking (stick and ball, green-carbon) conformations of compound **26** bound in the active site of PDE5A. Side chains of the protein are depicted as sticks, while metal molecules are represented as spheres. Key hydrogen bonds are represented as yellow dotted lines. **b** The best docking poses of compounds **1**–**43** clustered in the active site of PDE5A for a directly use to construct the QSAR models. Side chains of the protein are depicted as gray sticks, whereas the ligands are shown as green (compounds **1**–**11** and **24**–**43** in Q2 subpocket) or magenta (compounds **10**–**23** in a surface area) carbon based on the position of the C3-substituents. Pymol was used to prepare this figure (DeLano W.L., 2002)

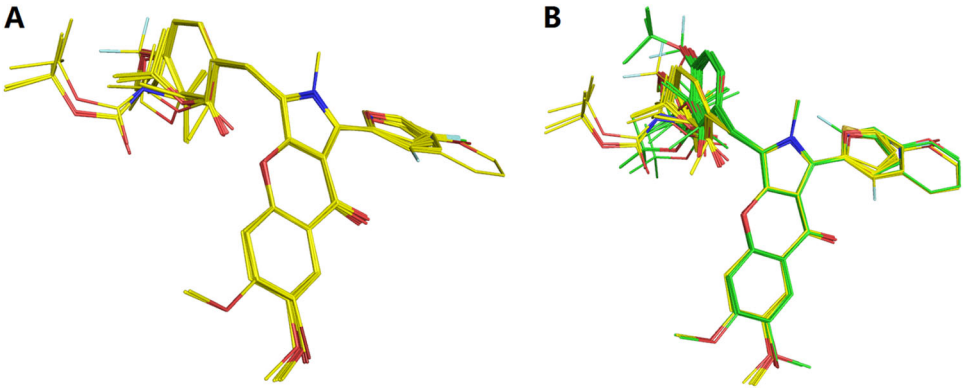

Fig. 2 Compounds **1**–**43** superimposed using atom-fit method. **a** Superimposed view of ligand-based alignment. **b** Comparison between the ligand-based alignment (yellow) and atom-fit superimposed docking poses used in the receptor-based alignment (green)

Table 2 Statistics of CoMFA and CoMSIA PLS analyses

Models	ONC	q^2	r^2	SEE	F	Field contributions (%)				
						S	E	H	D	A
Receptor-based alignment (RBA)										
CoMFA	4	0.630	0.959	0.196	193.563	51.9	48.1			
CoMSIA										
S+E	4	0.654	0.924	0.267	100.612	28.7	71.3			
E+H	5	0.632	0.938	0.246	96.327		51.9	41.8		
S+E+H	5	0.645	0.944	0.233	107.545	18.9	48.4	32.7		
S+E+A	3	0.641	0.891	0.315	92.640	23.7	43.6			32.7
E+H+A	5	0.589	0.950	0.220	121.160		42.3	29.1		28.6
S+E+H+A	5	0.611	0.953	0.214	129.468	12.0	38.9	24.0		25.1
S+E+H+A+D	3	0.596	0.897	0.307	98.3488	15.8	27.5	22.5	15.8	18.5
Ligand-based alignment (LBA)										
CoMFA	5	0.501	0.842	0.391	34.065	73.1	26.9			
CoMSIA										
S+E	6	0.404	0.802	0.445	20.915	48.3	51.7			
E+H	3	0.427	0.691	0.531	25.300		27.1	72.9		
S+E+H	3	0.435	0.706	0.517	27.232	20.0	22.1	57.9		
S+E+A	3	0.538	0.756	0.472	35.022	16.2	23.3			60.5
E+H+A	3	0.583	0.769	0.459	37.675		15.4	35.4		49.2
S+E+H+A	3	0.570	0.768	0.459	37.607	10.4	14.0	31.6		44.0
S+E+H+A+D	3	0.598	0.706	0.517	27.232	7.8	12.2	27.6	20.3	32.1

ONC Optimum number of components, q^2 Cross-validated correlation coefficient, r^2 Conventional non-cross validated correlation coefficient, *SEE* Non-cross validated standard error of estimate, *F* Fisher's *F*-value, *S* Steric, *E* Electrostatic, *H* Hydrophobic, *A* Hydrogen bond acceptor, *D* Hydrogen bond donor

dramatically less activities of compounds **12**–**20** from group A and **21**–**23** from group B.

To find out an effective alignment of this data set, molecules in the training and test sets were also subjected to a traditional LBA by superimposition on compound **26**. This type of alignment is relatively simple and fast, but often fails to take into account the three-dimensional nature of chemical structures. Its result is shown in Fig. 2a. A comparison of the two alignments illustrated that the major difference between them is the spatial arrangement of the substituents on pyrrol C3-position. Pyrrol C3-substitutens of RBA would have different directions and positions as discussed above, whereas those of LBA were aligned with a similar orientation to give rise to a perfect superimposition.

CoMFA and CoMSIA models generated from RBA and LBA methods

The CoMFA and CoMSIA results for the training set are listed in Table 2. In both CoMFA and CoMSIA analyses,

3D-QSAR models generated with the LBA are not as robust as the models based on the RBA. RBA CoMFA model generated a cross-validated coefficient (q^2) of 0.630, regression coefficient (r^2) of 0.959, and *F*-statistic value (F) of 193.563 at optimal number of components (ONC) of 4, while q^2, r^2, *F*, and ONC values obtained from the LBA method were 0.501, 0.842, 34.0605, and 5, respectively. Apparently, only RBA produced a significant CoMFA model, according to the usual criterion of reliability in QSAR studies ($q^2 \geq 0.5$ and $r^2 \geq 0.9$) (Fang et al., 2011; Golbraikh and Tropsha 2002; Tan et al., 2017; Zheng et al., 2017). RBA and LBA have each constructed seven CoMSIA models by using different combinations of steric (S), electrostatic (E), hydrophobic (H), hydrogen bond donor (D), and acceptor (A) fields to explore the impact of different fields on the reliability of the models. Almost all the RBA CoMSIA models were reasonable with q^2 values ranging from 0.589 to 0.654, and r^2 values of 0.897 to 0.953, whereas no significant LBA models were built (q^2 from 0.404 to 0.598, r^2 from 0.691 to 0.802). The CoMSIA-SE obtained from RBA was associated with highest q^2 and r^2 values, which has a q^2 of 0.654 and an r^2 of 0.924. Four components were used in the model building, and *F* value and standard error of estimate (SEE) for the non-cross-validation was 100.612 and 0.267, respectively. The high q^2, r^2, and *F* values together with the low SEE value indicated that this model is reliable and should have a good predictive ability. According to the CoMSIA-SE model, the steric and electrostatic contributions were 28.7% and 71.3%, respectively, which suggested that the electrostatic descriptor had more impact on compounds' biological activities than steric fields.

Ligand-based and RBAs are the most popular strategies used for CoMFA and CoMSIA QSAR studies to correlate biological activities with structural changes. In an earlier work, a remarkably higher cross-validated q^2 and the conventional r^2 values were obtained from a training set of 123 PDE9 agents using RBA method, compared with LBA method (Tan et al., 2017). Apparently, the statistical findings obtained in the present study suggested RBA also performed better than LBA in our PDE5 inhibitors QSAR studies. The RBA method is usually considered to be superior in searching the bioactive conformation for the ligand, which is crucial for the QSAR model generation. However, due to the rigid scaffold of aryl chromeno-pyrrol analogs, conformations used for RBA and LBA QSAR models were found to be almost similar as evident from the atom-fit superimposed docking poses (Fig. 2b), which suggested that it's not the conformation selection that plays an essential role in determining the reliability of our QSAR model. This hypothesis was confirmed by the failure of this alignment in constructing robust CoMFA and CoMSIA QSAR models (data not show). Comparison of the two alignments showed above that those compounds with long substituents on the pyrrol C3-position would have different spatial arrangements in the two alignments, although they have similar conformations, which may contribute to their different QSAR results.

External test set validation

The CoMFA and CoMSIA models for RBA and LBA were tested for their predictive ability on an external dataset of 5 diverse molecules. The predictive correlation coefficient (q^2_{pred}), the conventional correlation coefficient (r^2_{pred}) and the trend line slope (*k*) of the test for the two alignments are given in Table 3. Almost all the models of RBA produced statistical parameters meet the requirement for a robust model (q^2_{pred} value ≥ 0.5, r^2_{pred} value ≥ 0.9, and $0.85 \leq k \leq 1.15$). These satisfied results indicated that RBA could adequately account for the interactions between aryl chromeno-pyrrol analogs and PDE5. However, no decent results were obtained from the LBA, which is an indication of inherent defect of the simple LBA in interactions modeling. With the best RBA CoMSIA-SE model, q^2_{pred} of 0.854, r^2_{pred} of 0.953, and *k* of 0.997 were obtained. Comparisons of the predicted and experimental pIC_{50} values for CoMSIA-SE model are list in Table 1, and the scatter plot is shown in Fig. 3. It can be clearly seen that

Table 3 Predictive evaluation of the test set

Models	q^2	r^2	*k*
Receptor-based alignment (RBA)			
CoMFA	0.881	0.972	1.185
CoMSIA			
S+E	0.854	0.953	0.997
E+H	0.947	0.982	0.866
S+E+H	0.929	0.978	0.985
S+E+A	0.753	0.918	0.924
E+H+A	0.815	0.938	0.954
S+E+H+A	0.822	0.945	1.020
S+E+H+A+D	0.722	0.803	0.893
Ligand-based alignment (RBA)			
CoMFA	0.840	0.927	0.770
CoMSIA			
S+E	0.653	0.913	0.808
E+H	0.105	0.771	0.612
S+E+H	0.215	0.812	0.694
S+E+A	0.651	0.925	0.805
E+H+A	0.237	0.829	0.818
S+E+H+A	0.264	0.833	0.825
S+E+H+A+D	0.285	0.838	0.833

q^2 Predictive correlation coefficient of test, r^2 Conventional correlation coefficient of test, *k* Trend line slope of test

deviations between the predicted and experimental pIC_{50} values are in the acceptable range (<0.65 log unit).

Contour plots of the CoMSIA/SE model

The steric and electrostatic contour maps derived from the best RBA CoMSIA-SE model are illustrated in Fig. 4, where the favored and disfavored levels were set at 80% and 20%, respectively. The green and yellow contours shown in Fig. 4a indicate the areas where bulky substituents are favorable and disfavored to increase inhibitory activity, respectively. Figure 4b shows the electrostatic contour maps in which the blue and red contours represent that electrostatically positive and negative groups can enhance the biological activity at this region, respectively (Fig. 4b).

Figure 4a shows a green contour on the tyrosyl group of pyyrrol C3-position, which is surrounded by Val782, Ala783, Phe787, Ile813, and Met816 forming the lipophilic Q2 subpocket. It could explain why compounds with alkyl substituents at pyyrrol C3-position (**1**–**20**, group A) were usually less potent than C3-aromatic analogs (**21**–**43**, group B) against PDE5. However, there are limits to the size of this binding pocket, and too bulk substituents at this position can't be accommodated by it. Thus, these compounds have no choice but to escape to a surface area of the protein, the sterically disfavored region suggested by a big yellow contour, where little strong interactions can be formed (Fig. 2b). This hypothesis is clearly supported by a comparison of the average bioactivities of compounds **12**–**23** (average $pIC_{50} = 5.602$) with compounds **1**–**7** and **24**–**43** (average $pIC_{50} = 7.008$). In addition, there is a yellow region close to the position of C7, indicating that bulk groups will be disfavored at this position, which can be verified by the fact that the methoxyl substituent (compound **12**) confer an activity disadvantage over the corresponding methyl group (compound **13**).

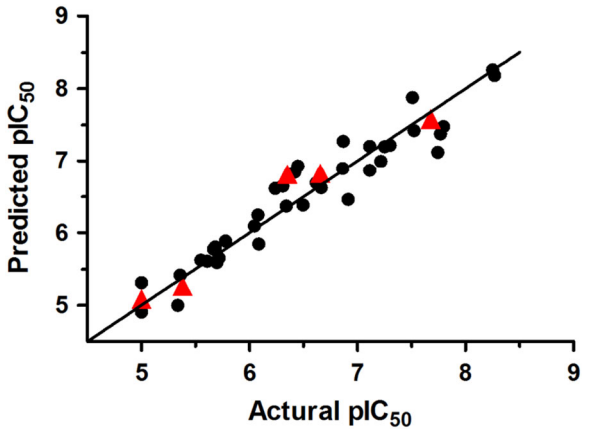

Fig. 3 Plots of predicted vs. actual pIC_{50} values of the training (black dot) and test sets (red triangle) for the CoMSIA/SE model generated form receptor-based alignment. The solid black line showed a perfect linear relationship (slope = 1) for reference

In Fig. 4b, a blue contour is observed close to the carboxyl group of compound **9**, indicating that electropositive groups at this position are favorable to increase the inhibitory potency of aryl-chromeno-pyrrol analogs. It was thus observed that the presence of electronegative carboxyl group here results in the loss of activities of compounds **8**–**11** from group A, although their carboxyl groups enter the Q2 subpocket. The blue contours on the N position of C3-pyridinyl of compound **37**, revealed that the electropositive groups at this position will increase the activity of the compounds, while electronegative group lowers the activity of compound **37**, compared with compound **30**. In addition, the blue contour appears on the core suggested electropositive group is required at this position. The aryl-chromeno-pyrrol core of less active compounds **25** and **31**–**33** from group B move away from the blue contour and does not sandwich perfectly with the side chain of Phe820 and Val782, which significantly lowers the activities of these compounds. These compounds have substituted phenyl group on the C1-position, which would push the core away from the sandwich place due to the limits of SP1 pocket.

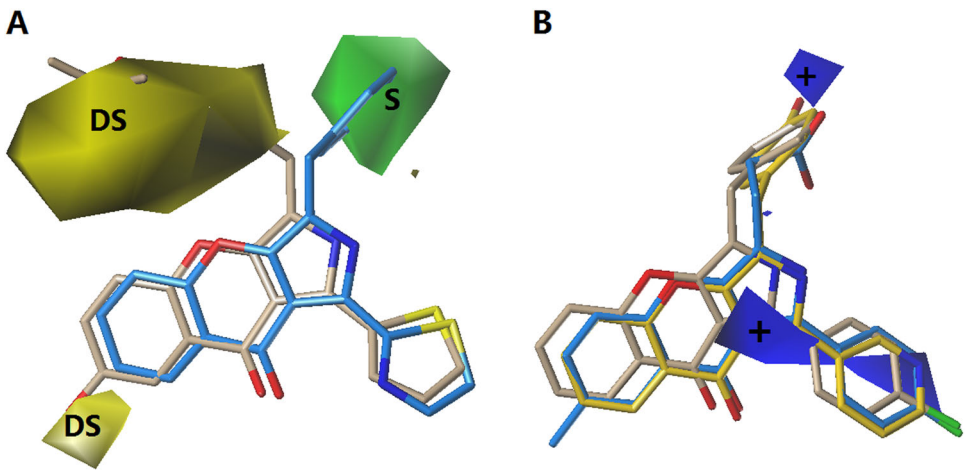

Fig. 4 Steric (**a**) and electrostatic (**b**) fields for receptor-based CoMSIA/SE model. Green/yellow contours indicate regions where steric bulky groups increase/decrease activity, while red/blue ones represent negative charge will increase/decrease activity. Favored and disfavored levels of these displayed fields are set at 80% and 20%, respectively. Representative compounds are depicted as sticks in blue (**26** and **9**), gray (**23** and **25**), or yellow (**37**) carbon

Concluding remarks

Reasonable alignment of the molecules plays a pivotal role in construction of significant 3D-QSAR models. Herein, the RBA is superior to the traditional LBA, giving more significant statistics results for 38 training set compounds and 5 test set molecules. Comparing the two alignments, the RBA generated a better spatial arrangement for the ligands within the active site of PDE5. The CoMSIA-SE contour maps suggested that aryl substitutes with suitable size both on C3 and at C1 position of the core are required to boost the potency of the compounds. In conclusion, the 3D-QSAR models on aryl-chromeno-pyrrol analogs as PDE5 inhibitors would provide valuable guidance for the design of novel PDE5 inhibitors with higher affinities.

Acknowledgements This work was supported by the Natural Science Foundation of China (81602968); the Natural Science Foundation of Guangdong Province (2016A030313589); the Medical Scientific Research Foundation of Guangdong Province (A2016201); and Science and Technology Program of Guangzhou, China (201707010049); Guangdong provincial Project (2016A020226018).

Compliance with ethical standards

Conflict of interest The authors declare that they have no conflict of interest.

References

Andersson KE (2018) PDE5 inhibitors—pharmacology and clinical applications 20 years after sildenafil discovery. Br J Pharmacol 175:2554–2565

Azzouni F, Abu SK (2011) Are phosphodiesterase type 5 inhibitors associated with vision-threatening adverse events? A critical analysis and review of the literature. J Sex Med 8:2894–2903

Champion HC, Bivalacqua TJ, Takimoto E, Kass DA, Burnett AL (2005) Phosphodiesterase-5A dysregulation in penile erectile tissue is a mechanism of priapism. Proc Natl Acad Sci USA 102:1661–1666

Corbin JD, Beasley A, Blount MA, Francis SH (2005) High lung PDE5: a strong basis for treating pulmonary hypertension with PDE5 inhibitors. Biochem Biophys Res Commun 334:930–938

DeLano W.L. (2002) The PyMOL Molecular Graphics System. DeLano Scientific, San Carlos, CA, USA

Discovery Studio 2. 5.5 (2009). Accelrys Inc., San Diego, CA, USA

Fang JS, Huang DN, Zhao WX, Ge H, Luo HB, Xu J (2011) A new protocol for predicting NovelGSK-3 ATP competitive inhibitors. J Chem Inf Model 51:1431–1438

Francis SH, Blount MA, Corbin JD (2011) Mammalian cyclic nucleotide phosphodiesterases: molecular mechanisms and physiological functions. Physiol Rev 91:651–690

Golbraikh A, Tropsha A (2002) Beware ofq2! J Mol Graph Model 20:269–276

Jung JY, Kim SK, Kim BS, Lee SH, Park YS, Kim SJ, Choi C, Yoon SI, Kim JS, Cho SD, Im GJ, Lee SM, Jung JW, Lee YS (2008) The penile erection efficacy of a new phosphodiesterase type 5 inhibitor, mirodenafil (SK3530), in rabbits with acute spinal cord injury. J Vet Med Sci 70:1199–1204

Keating GM, Scott LJ (2003) Vardenafil: a review of its use in erectile dysfunction. Drugs 63:2673–2703

Khan AS, Sheikh Z, Khan S, Dwivedi R, Benjamin E (2011) Viagra deafness—sensorineural hearing loss and phosphodiesterase-5 inhibitors. Laryngoscope 21:1049–1054

Kuschner WG (2005) Sildenafil citrate therapy for pulmonary arterial hypertension. N Engl J Med 353:2148–2157

Li L, Chen W, Chen T, Ren J, Xu Y (2016) Structure-based discovery of PDEs inhibitors. Curr Top Med Chem 16:917–933

Oh TY, Kang KK, Ahn BO, Yoo M, Kim WB (2000) Erectogenic effect of the selective phosphodiesterase type 5 inhibitor, DA-8159. Arch Pharm Res 23:471–476

Ribaudo G, Pagano MA, Bova S, Zagotto G (2016) New therapeutic applications of phosphodiesterase 5 inhibitors (PDE5-Is). Curr Med Chem 23:1239–1249

Rotella DP (2002) Phosphodiesterase 5 inhibitors: current status and potential applications. Nat Rev Drug Discov 1:674–682

Sakamoto T, Koga Y, Hikota M, Matsuki K, Murakami M, Kikkawa K, Fujishige K, Kotera J, Omori K, Morimoto H, Yamada K (2014) The discovery of avanafil for the treatment of erectile dysfunction: a novel pyrimidine-5-carboxamide derivative as a potent and highly selective phosphodiesterase 5 inhibitor. Bioorg Med Chem Lett 24:5460–5465

Scaglione F, Donde S, Hassan TA, Jannini EA (2017) Phosphodiesterase type 5 inhibitors for the treatment of erectile dysfunction: pharmacology and clinical impact of the sildenafil citrate orodispersible tablet formulation. Clin Ther 39:370–377

Shang NN, Shao YX, Cai YH, Guan M, Huang M, Cui W, He L, Yu YJ, Huang L, Li Z, Bu XZ, Ke H, Luo HB (2014) Discovery of 3-(4-hydroxybenzyl)-1-(thiophen-2-yl)chromeno[2,3-c] pyrrol-9(2H)-one as a phosphodiesterase-5 inhibitor and its complex crystal structure. Biochem Pharmacol 89:86–98

Sybyl 7.3 (2006). Tripos Associates, St. Louis, Missouri, USA

Tan C, Wu Y, Shao Y, Luo H, Zheng X, Wang L (2017) Docking-based 3D-QSAR studies of phosphodiesterase 9A inhibitors. Lett Drug Des Discov 14:986–998

Udeoji DU, Schwarz ER (2013) Tadalafil as monotherapy and in combination regimens for the treatment of pulmonary arterial hypertension. Ther Adv Respir Dis 7:39–49

Unegbu C, Noje C, Coulson JD, Segal JB, Romer L (2017) Pulmonary hypertension therapy and a systematic review of efficacy and safety of PDE-5 inhibitors Pediatrics 139:e20161450

Wu D, Zhang T, Chen Y, Huang Y, Geng H, Yu Y, Zhang C, Lai Z, Wu Y, Guo X, Chen J, Luo HB (2017) Discovery and optimization of Chromeno[2,3-c]pyrrol-9(2H)-ones as novel selective and orally bioavailable phosphodiesterase 5 inhibitors for the treatment of pulmonary arterial hypertension. J Med Chem 60:6622–6637

Zheng X, Wu Y, Wu D, Wang X, Zhang C, Guo X, Luo HB (2016) 3D-QSAR studies of 3-(3,4-dihydroisoquinolin-2(1H)-ylsulfonyl)benzoic acids as AKR1C3 inhibitors: highlight the importance of molecular docking in conformation generation. Biorg Med Chem Lett 26:5631–5638

Zheng X, Zhou S, Zhang C, Wu D, Luo HB, Wu Y (2017) Docking-assisted 3D-QSAR studies on xanthones as alpha-glucosidase inhibitors. J Mol Model 23:272